Unrefined montmorillonite nanoclay-cinnamon wood biochar composite for simultaneous removal of hardness and fluoride in groundwater

M.S.K. Ranaweera
Ecosphere Resilience Research Centre, Faculty of Applied Science, University of Sri Jayewardenepura, Nugegoda 10250, Sri Lanka
sashikamran@gmail.com

K. Karthika
National Water Supply and Drainage Board, Galle Road, Rathmalana, Sri Lanka
karthuk17@yahoo.com

S. Niruparan
Department of Engineering Technology, Faculty of Technology, University of Jaffna, Ariviyalnagar, Kilinochchi, Sri Lanka
niruparan@univ.jfn.ac.lk

M.Vithanage
Ecosphere Resilience Research Centre, Faculty of Applied Science, University of Sri Jayewardenepura, Nugegoda 10250, Sri Lanka
meththika@sjp.ac.lk

B.C.L. Athapattu
Centre for Environmental Studies and Sustainable Development (CESSD), The Open University of Sri Lanka, Nawala, Nugegoda, Sri Lanka
bcliy@ou.ac.lk

Abstract— **It was aimed to synthesize an adsorbent for fluoride and hardness removal using a nanoclay-biochar composite from unrefined Montmorillonite (MMT) clay from the Murunkan in Mannar, Sri Lanka. Fourier Transform Infrared Spectroscopy (FTIR), X-Ray Diffraction (XRD), X-Ray Fluorescence (XRF), Scanning Electron Microscope (SEM), and Thermal Gravimetric Analysis (TGA) were employed to characterize the materials. FTIR, XRD, and TGA analyses indicated the presence of MMT clay mineral in the sample. The SEM image of the composite confirmed the successful binding of MMT onto the biochar through a flaky appearance along the porous morphology. Further, the surface texture of clay and biochar could support hardness and fluoride removal by enhancing adsorption. The results obtained from CHN analysis show that the biochar sample was rich in carbon, which helps in the sorption of hardness and fluoride. The adsorption isotherm data of all the adsorbents were well fitted to the Temkin isotherm model, suggesting that the removal of hardness and fluoride onto the adsorbent indicates a heat of sorption. The kinetic adsorption data of all the adsorbents were well fitted to the pseudo-first-order kinetic model, indicating the dominant contribution of the physisorption mechanism. However, since the measured adsorption was minimal, a modification to the nanoclay-biochar composite is required for higher sorption efficiency by enhancing the active sites on sorbents to purify groundwater that contains an undesirable level of selected contaminants.**

Keywords: Montmorillonite nanoclay, Murukkan clay, biochar, nanocomposite, adsorption

I. Introduction

Chronic Kidney Disease of unknown etiology (CKDu) has been identified as a significant non-communicable disease in North Central Province (NCP) due to its high prevalence and public health effects. Over the past three decades, many investigations have taken place in the NCP of Sri Lanka concerning CKDu. The highest numbers of CKDu patients are recorded in the Anuradhapura district (Ranasinghe et al., 2024). The Ministry of Health conducted community-based screening programmes in 2015 and 2016, a total of 24,806 patients were identified from 11 districts designated as high risk for CKDu, of which 9,902 were from the Anuradhapura district (Senanayake, 2018).

Fluoride and hardness are factors contributing to the occurrence of CKDu, and fluoride content associated with hardness is a significant hydrogeochemical feature in all regions of CKDu studied (Wickramarathna et al., 2017). Moreover, Liyanage et al., (2022) found that fluoride ions and water hardness associated with higher Mg^{2+} ions may influence CKDu.

In accordance with the Water Quality Association (WQA) and the United States Geological Survey (USGS), hard water is classified according to its Ca2+ and Mg2+ ion concentration in water: 0–60 mg/L is considered soft water, 61–120 mg/L is considered moderately hard water, 121-180 mg/L is considered hard water and more than 180 mg/L is considered very hard water. Total water hardness includes carbonate and non-carbonate hardness, primarily associated with Ca^{2+} and Mg^{2+} ions (Shmeis, 2018).

Drinking water containing fluoride can also have positive and negative effects on human health. As one of the suspected chemical contaminants that cause CKDu in Sri Lanka, fluoride is widely distributed in the environment. In areas affected by CKDu in Sri Lanka, groundwater contains unsafe levels of fluoride (Paranagama et al., 2018). In more than 98% of CKDu patients, groundwater is their primary water source, and fluoride interactions in groundwater cause the disease (Hettithanthri et al., 2021). There are higher fluoride concentrations in the dry zone groundwater of the NCP (0.2–8 mg/L) than in the wet zone (0.2–0.8 mg/L) in Sri Lanka. Because of high fluoride levels in both the soil and groundwater, crops grown in NCP contain higher fluoride concentrations (Paranagama et al., 2018).

A higher fluoride concentration is associated with a higher hardness concentration in groundwater from CKDu regions compared to non-CKDu regions, and this enhances CKDu. Long-term and continuous exposure to fluoride and hardness in drinking water could enhance the damage by further causing renal failure at an end-stage (Wickramarathna et al., 2017).

To improve the quality of life, it is imperative that these contaminants be removed from drinking water. Water can be treated using many methods, including adsorption, precipitation (Pakharuddin et al., 2021), ion exchange, reverse osmosis (Tayeh, 2024), electrochemical treatments (Alkhadra et al., 2022), membrane filtration, and bio-sorption (Mutegoa, 2024). Among those, adsorption is relatively inexpensive, easy to design, easy to perform, highly efficient, eco-friendly, and produces fewer toxic intermediates. Furthermore, most adsorbents used in adsorption studies are abundant, naturally derived, and relatively inexpensive, such as biochar and clay (Zaman et al., 2023).

Clay-biochar composites have been studied for various environmental applications since both materials possess good adsorption capability. However, clay-biochar composites were considered potential adsorbents of several contaminants (Chaukura et al., 2020). There were no studies conducted on the removal competencies of hardness and fluoride. Hence, this research aims to assess the performance of nanocomposites for the removal efficiency of hardness and fluoride in groundwater using locally available nanoclay and biochar.

II. EXPERIMENTAL

A. Materials and chemicals

The clay sample was collected from the Murunkan, composed of soil with higher MMT content (Piyasena et al., 2019) in the Mannar district of Northwestern Province in Sri Lanka. Biochar was produced from the pyrolysis of Cinnamon wood. All solutions were prepared using deionized water. 2 mg/L synthetic solutions of fluoride were prepared with Sodium Fluoride, and 500 mg/L synthetic solutions of hardness were prepared with Calcium Chloride and Magnesium Chloride.

B. Clay and biochar preparation

To remove any organic and coarse particles present in the clay, a wet sieve analysis was performed on the collected sample from 63 µm sieve. Afterwards, the specimen was dried at 110 °C in an oven. The dry specimen was ground to make the powder, and a dry sieve analysis was performed using from 63 µm sieve. It was heated up to 300 °C for 1 hour to remove organic materials from the clay sample (Wanasinghe & Adikary, 2017). The Cinnamon wood was collected and air-dried overnight. Then the sample was pyrolyzed at 600 °C for 1 hour under oxygen-limited conditions (Yao et al., 2014). The resulting chars were allowed to cool to room temperature. Afterwards, the biochar sample was crushed and sieved to remove particles larger than 63 µm.

C. Characterization of clay and biochar

The resultant sample was subjected to Fourier Transform Infrared Spectroscopy (FTIR), X-Ray Diffraction (XRD), and Thermal Gravimetric Analysis (TGA) to verify the presence of MMT. XRF analysis of clay and biochar samples was carried out to identify the chemical composition. Scanning Electron Microscope (SEM) Analysis was carried out to determine the MMT clay structure in the clay sample. In addition, the SEM analysis was carried out for biochar to identify the morphology of the biochar structure. CHN analysis of the biochar sample was carried out to determine the carbon, hydrogen, and nitrogen elemental concentrations. These analyses for the clay and biochar samples were carried out at the Sri Lanka Institute of Nanotechnology (Pvt) Ltd, Sri Lanka.

D. Adsorption studies

The clay-biochar composites were prepared using clay and biochar in the form of balls for three selected different mixing proportions (1:1, 2:1, 3:1) with an average diameter of 5mm. The heat treatment process was carried out at 1000 °C for 7 hours to improve the stability of the clay-biochar composite (Mahalekam et al., 2016). And also, clay adsorbent was prepared using clay in the form of balls. However, biochar was used in powder form. The 20 ml samples were sequentially collected from the shaker after 0, 15, 30, 60, and 120 min at natural pH for the adsorbent to determine fluoride and hardness adsorption capacities onto the 4 g of adsorbents. In addition, 28 °C temperature and 80 rpm stirring speed were used as other operating parameters of the shaker.

1) Sorption Isotherm

Non-linear models such as Langmuir (1), Freundlich (2), Temkin (3), and Dubinin-Radushkevich (4) were used to fit experimental isotherm data and which helps to understand the physico-chemical mechanism of the adsorbents and adsorption process at the solid-liquid interface.

$$q_e = \frac{Q.K_L C_e}{1+K_L C_e} \quad (1)$$

$$q_e = K_f C_e^{\frac{1}{n}} \quad (2)$$

$$q_e = \frac{RT}{b_T} \ln A_T C_e \quad (3)$$

$$q_e = q_s.exp(-B \in^2) \quad (4)$$

Where C_e represents the equilibrium concentration (mg/L), K_L represents the Langmuir equilibrium constant (L/mg), q_e represents the adsorbed amount per adsorbent amount (mg/g), Q represents the Langmuir maximum adsorption capacity (mg/g), and n and K_f are Freundlich constants related to nonlinear adsorption, R represents the universal gas constant (8.314 J/mol.K), A_T represents the Temkin isotherm equilibrium-binding constant (l/g), b_T represents the Temkin isotherm constant, q_s represents the theoretical isotherm saturation capacity (mg/g), B represents the Dubinin-Radushkevich isotherm constant (mol2.k/J2), ϵ represents the Dubinin-Radushkevich isotherm constant (potential energy) (Girish, 2017).

2) Sorption Kinetics

Models based on non-linear kinetics, such as pseudo-first order (5) and pseudo-second order (6), were used to explain the mechanisms of hardness and fluoride adsorption onto biochar, clay, and composite adsorbents.

$$q = q_e(1 - e^{k_1 t}) \tag{5}$$

$$q = \frac{k_2 {q_e}^2 t}{1 - k_2 q_e t} \tag{6}$$

Where qt represents the amount adsorbed at time t, q_e represents the equilibrium amount, t represents the time in minutes, and k_1 and k_2 represent the rate constants of the pseudo-first and pseudo-second order models, respectively (Batool et al., 2018).

E. Column experiment

The nanoclay fraction of the sample was isolated using the combination of sedimentation and centrifuging with the addition of sodium chloride (NaCl). First, the nanocomposites were prepared using nano clay and biochar in the form of balls using selected mixing proportions with an average diameter of 5 mm. The filter was filled with 3 g of nanoclay-biochar composite, and then a 150 ml water sample was poured manually and collected at the bottom of the column. Before treating the water samples, it was washed using deionized water. Figure 1 shows the experimental column setup used to treat water samples.

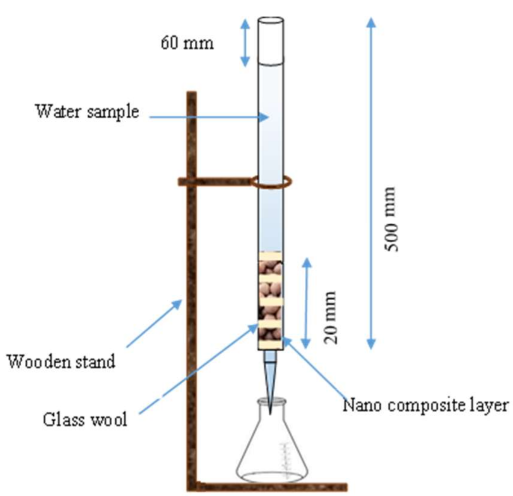

Figure 1. Experimental column setup.

III. Results and Discussion

A. Characterization of raw samples

1) FTIR analysis

FTIR spectra for clay specimens are given in Figure 2. revels characteristic peak at 3384 cm^{-1} is due to the –OH stretching band. An absorption peak around 1635 cm^{-1} is caused by –OH stretching in adsorbed water, and the characteristic peak at 1413 cm^{-1} is caused by Si–O stretching.

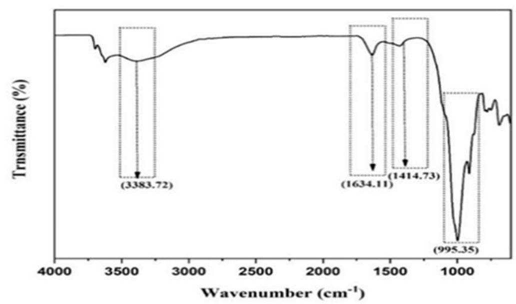

Figure 2. FTIR spectrum of the clay sample

The peak at 995 cm^{-1} is the result of the stretching of Si–O in layered silicates (Madejova & Komadel, 2001; Patel et al., 2006). MMT spectra are characterized by OH stretching at 3650 cm^{-1} and Si-O stretching at 1050 cm^{-1} (Ashiq et al., 2019). However, when considering the literature, it is verified that the clay sample consists of MMT clay mineral.

2) XRD analysis

The interlaminar distance d (001) was calculated using Bragg's law, and XRD measured the 2θ angle. The XRD pattern of the MMT sample showed shape peaks for X-ray reflections at 2θ values 20.99° (d=4.23), 26.49° (d=3.36), and 36.49° (d=2.46) in Figure 3. There were four peaks associated with MMT are 13.6 Å, 4.47 Å, 3.13 Å, and 2.56 Å (Peter, 1986). The maximum intensity peak was recorded for MMT, and more peak values were indicated for MMT than for other minerals. It can be verified that the clay sample consists of MMT clay based on the spacing values (d values) in the specimen and d values in the literature for MMT clay.

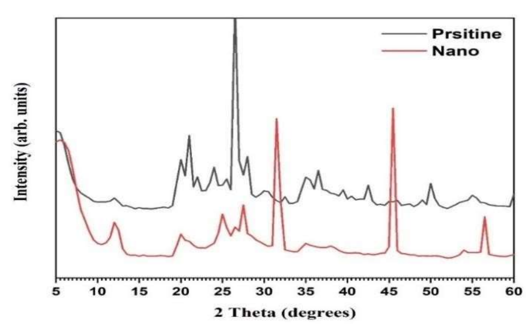

Figure 3. XRD patterns of for MMT sample and the isolated Nano MMT sample

The XRD pattern of the nano MMT sample showed major X-ray reflections at 27.49° (d=3.24), 31.49° (d=2.84), 45.49° (d=1.99), and 56.49° (d=1.63). As compared to pristine clay, nanoclay peaks shifted at lower angles, indicating an increase in the interlayer distance from intercalation or exfoliation. The pristine clay particles in Figure 3 are relatively sharp and high compared to the nanoclay particles, which means that they are relatively more crystalline (Zyoud et al., 2016). The peaks 230 became shorter and broader for nanoclay.

3) TGA analysis

The result of the thermogravimetric analysis for the clay sample is shown in Figure 4.

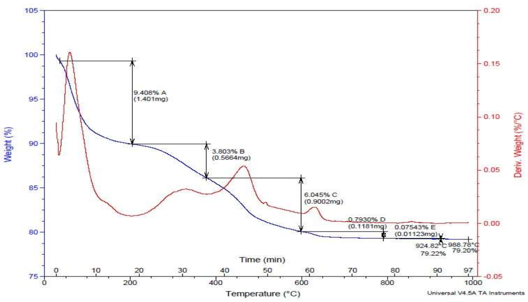

Figure 4. Thermal Analysis for the clay sample

MMT clay mineral and quartz will produce exothermic peaks after 1000 0C. MMT displays endothermic peaks between 650 and 700 ºC due to its hydroxyl group (Adikary & Wanasinghe, 2012). According to this pattern, there is a weight loss in that range. Hence, it can be verified that the clay sample consists of MMT clay minerals.

4) CHN analysis

Table I presents the CHN analysis of the biochar, showing a high carbon content of 71.27% and an O/C ratio of 0.30, which aligns with the typical range of 0.2–0.6 for biochar (Spokas, 2010). These values confirm that the cinnamon-derived sample is a carbon-rich biochar produced through efficient slow pyrolysis.

TABLE I. CHN RESULTS OF GASIFIED BIOCHAR

C	H	N	O	H/C	O/C
71.27	2.44	0.62	21.11	0.03	0.30

The H/C ratio of a biochar indicates its stability and aromaticity. The <0.1 molar H/C ratio in biochar indicated a more graphite-like structure (Denyes et al., 2014). Hence, cinnamon biochar is rich in aromatic graphite-like structure, expected to remove heavy metals and fluoride present in the drinking water.

Furthermore, a molar H/C ratio of ≤0.3 indicates highly condensed aromatic ring systems, whereas a molar H/C ratio of ≥ 0.7 suggests non-condensed structures. Hence, gasified biochar (having a molar H/C ratio of 0.03) may contain highly condensed aromatic rings in its structure. Nevertheless, a low molar H/C ratio indicates a higher degree of carbonization in biochar (Wood et al., 2024).

5) XRF analysis

The major chemical compositions of MMT and BC are summarized in Table II. Si, Fe, and Al were the significant elements, while other elements, Ca, K, Ti, Mn, and S, occurred as minor elements. MMT clay minerals have complex structures of Fe^{2+}, Fe^{3+}, Al^{3+}, $Mn^{3+,}$ and Mn^{2+} ions in octahedral sites embedded with cations like Si^{4+} and Al^{3+} in the tetrahedral sites (Muriithi et al., 2012).

Therefore, it is signified that MMT clay minerals were present in this clay sample. In the XRF results of biochar mass, K accounted as the major element with 86.61% of the mass. And other elements of Si, P, Fe, S, Ti, and Mn occurred as minor elements. As a result, the biochar was mainly composed of Ca, K, and Mg, with lesser amounts of Na, Mn, Ba, Fe, and Sr. Also, this biochar sample had experienced the shortest reactor residence times (Brewer et al., 2011).

6) SEM analysis

The SEM image of the clay sample shows a flake and plate-like appearance that is unique for MMT (Ashiq et al., 2019). So, considering the similar structures, it verifies that the MMT clay. SEM image of clay is shown in Figure 5 (a), and it can be noticed that the numerous pores in the image show the flaky clay structures embedded in the voids.

SEM analysis of the cinnamon biochar illustrates the smooth surface morphology of a porous structure with numerous hollow cells. Large channel-like structures proliferate on the surface of the biochar, showing at least partial retention of the morphology of the initial input biomass.

SEM image of biochar is shown in Figure 5 (b), and it displays a plane cleavage surface with broken edges, many alcoves, and protrusions (Fosso-kankeu et al., 2015).

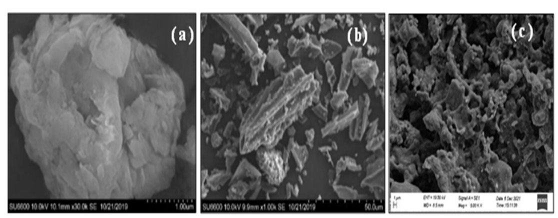

Figure 5. SEM images (a) Clay sample; (b) Biochar sample; (c) clay-biochar composite

.

TABLE II. CHEMICAL COMPOSITION OF MMT AND BC

Element	Al	Si	P	S	K	Ca	Ti	Mn	Fe
MMT%	-	7.47	2.74	2.01	84.65	-	0.66	0.44	2.02
BC%	17.10	55.53	-	0.28	2.88	3.68	2.06	0.33	18.13

Biochar produced at higher temperatures facilitated the release of volatile materials and created more pores, resulting in a larger surface area (Anyebe et al., 2025). A greater surface area is desirable because it aids in improving soil properties and increases water retention capacity to a greater extent (Wei et al., 2023).

The SEM image of the clay-biochar composite is shown in Figure 5 (c). The clay-biochar composite creates voids via impregnating biochar into clay, which helps to interact with selected contaminants for embedding into voids to enhance adsorption.

B. Characterization of nanoclay

The cumulative nano clay fraction percentage has fallen below 200 nm, revealing that the isolated clay fraction has considerable amounts of nanoparticles. Figure 6 represents the laser particle size analysis of isolated clay specimens.

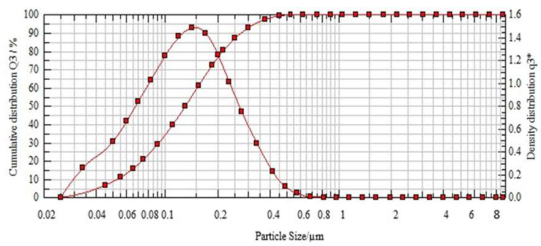

Figure 6. Laser particle size analysis of an isolated clay specimen

C. Adsorption studies

The removal efficiencies for each adsorbent were calculated with a 436 mg/L hardness concentration and 2.2 mg/L fluoride concentration. The variation of removal efficiencies of contaminants is shown in Figure 7.

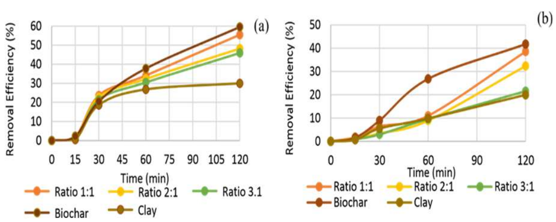

Figure 7. (a) The variation of fluoride removal efficiencies with time; (b) The variation of hardness removal efficiencies with time

Biochar has considerably higher fluoride and hardness adsorption capability than other adsorbents. However, powdered biochar is rather difficult to separate from the aqueous solution, thus making it practically unusable.

Then the next best adsorbent is the 1:1 clay-biochar composite. In clay-biochar composites, biochar acts as a good porous matrix for distributing clay particles within it. Then, clay-biochar composites have a lower surface area than biochar due to the clay particles clogging pores. However, biochar and clay perform well at removing contaminants, and their sorption has significantly increased; hence, the decreasing surface area does not result in a decrease in sorption (Rajapaksha et al., 2016).

This finding shows that clay and biochar are equally essential to obtain a promising result for removing contaminants. The negative surface explains the high adsorption capacity of clay-biochar composite, and then it possesses the cationic nature of hardness (Ca^{2+} and Mg^{2+}) than fluoride. The results of the hardness and fluoride on the adsorbents are denoted in Table III.

Measured adsorption isotherms and kinetic model parameters of hardness and fluoride onto tested adsorbents are shown in Table IV, and the Temkin isotherm model best describes the adsorption of hardness and fluoride by all adsorbents than other adsorption isotherm models. In addition, the Temkin model considers the interactions between contaminants and adsorbents, indicating a heat of sorption.

TABLE III. THE FLUORIDE AND HARDNESS ADSORPTION CAPACITY ONTO THE ADSORBENTS

Sample weight	Element	Mass%
Clay-biochar ratio 1:1	0.046	7.000
Clay-biochar ratio 2:1	0.040	5.875
Clay-biochar ratio 3:1	0.038	3.917
Biochar	0.049	7.583
Clay	0.025	3.625

The simplest cases are first-order adsorption, which is usually valid for physisorption, and second-order adsorption, which is usually valid for dissociative chemisorption (Pisarev, 2012). Among the two models, the pseudo-first-order model produced the best fit to the rapid stage of the adsorption reaction, with a correlation coefficient (R^2) value. Therefore, physisorption was revealed as the mechanism of adsorbate-adsorbent complexation in the kinetic model of adsorbate-adsorbent interaction.

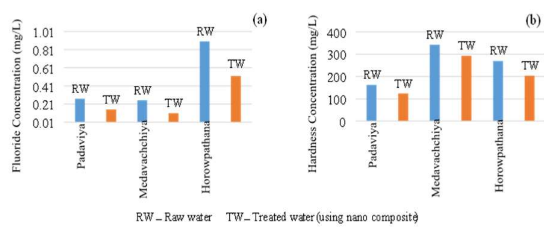

Figure 8. (a) The variation of fluoride concentration of collected water samples; (b) The variation of total hardness concentration of collected water samples

Figure 8 represents the variation of fluoride and hardness concentrations in the nanocomposite. It was noted that the percentage of removals (%) corresponds to the maximum hardness and fluoride concentrations in water samples collected in the Anuradhapura district.

In this study, the removal percentages were 56% for fluoride and 24.82% for hardness. The negative surface of the nanocomposite is responsible for its high adsorption capacity, which is attributed to the cationic nature of hardness (Ca^{2+} and Mg^{2+}).

TABLE IV. PSEUDO FIRST ORDER AND TEMKIN MODEL PARAMETERS FOR THE ADSORPTION OF HARDNESS AND FLUORIDE ONTO CLAY, BIOCHAR, AND CLAY-BIOCHAR COMPOSITES

	Model	Model Parameters	1:1	2:1	3:1	Biochar	Clay
Hardness	Pseudo First Order	q_e	2.478	2.293	2.038	2.989	2.013
		K_1	0.0496	0.0452	0.0817	0.1429	0.1013
		R^2	0.982	0.969	0.925	0.912	0.961
	Temkin	$B=RT/b_T$	2.083	1.788	1.246	2.513	1.129
		A_T	0.289	0.265	0.295	0.343	0.349
		R^2	0.998	0.999	0.999	0.995	0.999
Fluoride	Pseudo First Order	q_e	3.126	3.210	3.293	3.002	3.073
		K_1	0.147	0.171	0.168	0.147	0.334
		R^2	0.935	0.933	0.934	0.957	0.946
	Temkin	$B=RT/b_T$	0.0141	0.012	0.012	0.016	0.008
		A_T	0.436	0.469	0.466	0.399	0.584
		R^2	0.983	0.989	0.990	0.983	0.998

IV. CONCLUSIONS

The sample collected from the Murunkan in the Mannar district contains MMT, confirmed through XRF, FTIR, and TGA analysis. A peak at 995 cm^{-1} has been attributed to Si–O stretching for layered silicates, which facilitate the removal of hardness in water by forming bonds with the Si-O stretch. In SEM analysis, clay has a plate-like cross-section, which indicates a flaky structure unique to the MMT clay mineral, which enhances the removal of harness and fluoride.

Experiments indicated that the pseudo-first-order kinetics model fitted hardness and fluoride adsorption kinetics onto all adsorbents and that the Temkin model described adsorption isotherms well. MMT clay is most preferred to extract nanoparticles due to its high surface area and cation exchange capabilities. Therefore, the extracted MMT nanoclay was used to prepare a nanoclay-biochar composite. However, a modification should be carried out on MMT nanoclay-biochar composite for higher sorption efficiency by enhancing the active sites on the composites for treating contaminated water rich in hardness and fluoride. Then it could be a highly sustainable adsorbent as a low-cost and locally available option for treating contaminated water.

ACKNOWLEDGMENTS

The authors wish to acknowledge Lanka Mineral and Chemical (Pvt) Ltd for analytical support.

REFERENCES

[1] Adikary, S. U., & Wanasinghe, D. D. (2012). Characterization of locally available Montmorillonite clay using FTIR technique. *Annual Transactions of Institution of Engineers Sri Lanka 2*. www.sigmaaldrich.com,

[2] Alkhadra, M. A., Su, X., Suss, M. E., Tian, H., Guyes, E. N., Shocron, A. N., Conforti, K. M., de Souza, J. P., Kim, N., Tedesco, M., Khoiruddin, K., Wenten, I. G., Santiago, J. G., Hatton, T. A., & Bazant, M. Z. (2022). Electrochemical Methods for Water Purification, Ion Separations, and Energy Conversion. *Chemical Reviews*, *122*(16), 13547–13635. https://doi.org/10.1021/acs.chemrev.1c00396

[3] Anyebe, O., Sadiq, F. K., Manono, B. O., & Matsika, T. A. (2025). Biochar Characteristics and Application: Effects on Soil Ecosystem Services and Nutrient Dynamics for Enhanced Crop Yields. In *Nitrogen* (Vol. 6, Issue 2). https://doi.org/10.3390/nitrogen6020031

[4] Ashiq, A., Sarkar, B., Adassooriya, N., Walpita, J., Rajapaksha, A. U., Ok, Y. S., & Vithanage, M. (2019). Sorption process of municipal solid waste biochar-montmorillonite composite for ciprofloxacin removal in aqueous media. *Chemosphere*, *236*, 124384. https://doi.org/10.1016/j.chemosphere.2019.124384

[5] Batool, F., Akbar, J., Iqbal, S., Noreen, S., & Bukhari, S. N. A. (2018). Study of isothermal, kinetic, and thermodynamic parameters for adsorption of cadmium: an overview of linear and nonlinear approach and error analysis. *Bioinorganic Chemistry and Applications*, *2018*.

[6] Brewer, C. E., Unger, R., Schmidt-Rohr, K., & Brown, R. C. (2011). Criteria to select biochars for field studies based on biochar chemical properties. *Bioenergy Research*, *4*(4), 312–323.

[7] Chaukura, N., Chiworeso, R., Gwenzi, W., Motsa, M. M., Munzeiwa, W., Moyo, W., Chikurunhe, I., & Nkambule, T. T. I. (2020). A new generation low-cost biochar-clay composite 'biscuit' ceramic filter for point-of-use water treatment. *Applied Clay Science*, *185*(September 2019), 105409. https://doi.org/10.1016/j.clay.2019.105409

[8] Denyes, M. J., Parisien, M. A., Rutter, A., & Zeeb, B. A. (2014). Physical, chemical and biological characterization of six biochars produced for the remediation of contaminated sites. *Journal of Visualized Experiments : JoVE*, *93*, e52183. https://doi.org/10.3791/52183

[9] Fosso-kankeu, E., Waanders, F. B., & Steyn, F. W. (2015). *The Preparation and Characterization of Clay-Biochar Composites for the Removal of Metal Pollutants*. *December*. https://doi.org/10.15242/iie.e1115016

[10] Girish, C. R. (2017). Various isotherm models for multicomponent adsorption: A review. *International Journal of Civil Engineering and Technology*, *8*(10), 80–86.

[11] Hettithanthri, O., Sandanayake, S., Magana-Arachchi, D., Wanigatunge, R., Rajapaksha, A. U., Zeng, X., Shi, Q., Guo, H., & Vithanage, M. (2021). Risk factors for endemic chronic kidney disease of unknown etiology in Sri Lanka: Retrospect of water security in the dry zone. *Science of the Total Environment*, *795*, 148839. https://doi.org/10.1016/j.scitotenv.2021.148839

[12] J. Wimalawansa, S. (2016). Effect of Water Hardness on Non-Communicable Diseases, Including Chronic Kidney Disease of Multifactorial Origin (CKDmfo/CKDuo). *Journal of Environment and Health Science*, *2*(1), 1–11. https://doi.org/10.15436/2378-6841.16.029

[13] Jayarathne, D. L. S. M., Ariharan, S., Iqbal, S. S., & Thayaparan, M. (2015). Isotherm Study for the Biosorption of Cd (II) from Aqueous Solution by the Aquatic Weed: Ceratophyllum demersum. *Journal of Environmental Professionals Sri Lanka*, *4*(2), 10. https://doi.org/10.4038/jepsl.v4i2.7859

[14] Kajjumba, G. W., Emik, S., Öngen, A., Özcan, H. K., & Aydın, S. (2018). Modelling of adsorption kinetic processes—errors, theory and application. *Advanced Sorption Process Applications*, 0–19.

[15] Liyanage, D. N. D., Diyabalanage, S., Dunuweera, S. P., Rajapakse, S., Rajapakse, R. M. G., & Chandrajith, R. (2022). Significance of Mg-hardness and fluoride in drinking water on chronic kidney disease of unknown etiology in Monaragala, Sri Lanka. *Environmental Research*, *203*(July 2021), 111779. https://doi.org/10.1016/j.envres.2021.111779

[16] Madejova, J., & Komadel, P. (2001). Baseline studies of the clay minerals society source clays: infrared methods. *Clays and Clay Minerals*, *49*(5), 410–432.

[17] Mahalekam, M., Heshan, G. D. K., Wijayasinghe, H., & Balasooriya, N. W. B. (2016). *Determination of Zn2+ ion adsorption capacity of montmorillonite clay*.

[18] Muriithi, N. T., Karoki, K. B., & Gachanja, A. N. (2012). Chemical and mineral analyses of Mwea clays. *International Journal of Physical Sciences*, *7*(44), 5865–5869.

[19] Mutegoa, E. (2024). Efficient techniques and practices for wastewater treatment: an update. *Discover Water*, *4*(1), 69. https://doi.org/10.1007/s43832-024-00131-8

[20] Pakharuddin, N., Fazly, M., Sukari, S., Tho, K., & Zamri, F. (2021). Water treatment process using conventional and advanced methods: A comparative study of Malaysia and selected countries. *IOP Conference Series: Earth and Environmental Science*, *880*, 12017. https://doi.org/10.1088/1755-1315/880/1/012017

[21] Paranagama, D. G. A., Bhuiyan, M. A., & Jayasuriya, N. (2018). Factors associated with Chronic Kidney Disease of unknown aetiology (CKDu) in North Central Province of Sri Lanka: a comparative analysis of drinking water samples. *Applied Water Science*, *8*(6), 1–16. https://doi.org/10.1007/s13201-018-0792-9

[22] Patel, H. A., Somani, R. S., Bajaj, H. C., & Jasra, R. V. (2006). Nanoclays for polymer nanocomposites, paints, inks, greases and cosmetics formulations, drug delivery vehicle and waste water treatment. *Bulletin of Materials Science*, *29*(2), 133–145.

[23] Peter, B. (1986). *Mineral Powder Diffraction File, Search manual, Data book, Joint Committee on Powder diffraction Standards data cards (JCPDS), JCPDS International Center for Diffraction Data*. USA.

[24] Pisarev, A. A. (2012). Hydrogen adsorption on the surface of metals. In *Gaseous Hydrogen Embrittlement of Materials in Energy Technologies* (pp. 3–26). Elsevier.

[25] Piyasena, K., Rathnayake, S. I., & Pitawala, H. (2019). *Characterisation and Implications for Potential Environmental Applications of Montmorillonite Extracted from Clay Deposits in Murunkan, Sri Lanka*.

[26] Premarathna, K. S. D., Rajapaksha, A. U., Adassoriya, N., Sarkar, B., Sirimuthu, N. M. S., Cooray, A., Ok, Y. S., & Vithanage, M. (2019). Clay-biochar composites for sorptive removal of tetracycline antibiotic in aqueous media. *Journal of Environmental Management*, *238*(January), 315–322. https://doi.org/10.1016/j.jenvman.2019.02.069

[27] Rajapaksha, A. U., Chen, S. S., Tsang, D. C. W., Zhang, M., Vithanage, M., Mandal, S., Gao, B., Bolan, N. S., & Ok, Y. S. (2016). Engineered/designer biochar for contaminant removal/immobilization from soil and water: Potential and implication of biochar modification. *Chemosphere*, *148*, 276–291. https://doi.org/10.1016/j.chemosphere.2016.01.043

[28] Ranasinghe, A., Somatunga, L., Kumara, G., Karunarathna, R., De Silva, P., Gunawardena, J., Kumari, S., Sarjana, M., & de Silva, M. (2024). Decreasing incidence of hospital diagnosed CKD/CKDu in North Central Province of Sri Lanka: is it related to provision of drinking water reverse osmosis plants? *BMC Nephrology*, *25*. https://doi.org/10.1186/s12882-024-03534-w

[29] Senanayake, S. (2018). Chronic kidney disease in Sri Lanka: a glimpse into lives of the affected. *J Coll Community Physicians Sri Lanka*, *24*, 2.

[30] Shmeis, R. M. A. (2018). Water Chemistry and Microbiology. In *Fundamentals of Quorum Sensing, Analytical Methods and Applications in Membrane Bioreactors* (1st ed., Vol. 81). Elsevier B.V. https://doi.org/10.1016/bs.coac.2018.02.001

[31] Spokas, K. A. (2010). Review of the stability of biochar in soils: predictability of O: C molar ratios. *Carbon Management*, *1*(2), 289–303.

[32] Tayeh, Y. A. (2024). A comprehensive review of reverse osmosis desalination: Technology, water sources, membrane processes, fouling, and cleaning. *Desalination and Water Treatment*, *320*, 100882. https://doi.org/https://doi.org/10.1016/j.dwt.2024.100882

[33] Wanasinghe, D. D., & Adikary, S. U. (2017). Extraction and characterisation of Montmorillonite nano clay from Sri Lankan clay deposits. *2017 Moratuwa Engineering Research Conference (MERCon)*, 64–67. https://doi.org/10.1109/MERCon.2017.7980457

[34] Wei, B., Peng, Y., Lin, L., Zhang, D., Ma, L., Jiang, L., Li, Y., He, T., & Wang, Z. (2023). Drivers of biochar-mediated improvement of soil water retention capacity based on soil texture: A meta-analysis. *Geoderma*, *437*, 116591. https://doi.org/https://doi.org/10.1016/j.geoderma.2023.116591

[35] Wickramarathna, S., Balasooriya, S., Diyabalanage, S., & Chandrajith, R. (2017). Tracing environmental aetiological factors of chronic kidney diseases in the dry zone of Sri Lanka—A hydrogeochemical and isotope approach. *Journal of Trace Elements in Medicine and Biology*, *44*, 298–306. https://doi.org/10.1016/j.jtemb.2017.08.013

[36] Wood, R., Mašek, O., & Erastova, V. (2024). Developing a molecular-level understanding of biochar materials using public characterization data. *Cell Reports Physical Science*, *5*(7), 102036. https://doi.org/https://doi.org/10.1016/j.xcrp.2024.102036

[37] Xiang, L., Zhao, X., & Yin, J. (2011). Micro/nano-structured montmorillonite/titania particles with high electrorheological activity. *Rheologica Acta*, *50*(1), 87–95.

[38] Yao, Y., Gao, B., Fang, J., Zhang, M., Chen, H., Zhou, Y., Creamer, A. E., Sun, Y., & Yang, L. (2014). Characterization and environmental applications of clay–biochar composites. *Chemical Engineering Journal*, *242*, 136–143.

[39] Zaman, M., Safdar, M., Maqbool, Z., Shahid, M. A., Majeed, M. D., Muzammil, H., & Majeed, T. (2023). *Green Adsorbents for Water Purification* (M. M. M. Elnashar & S. Karakuş (eds.)). IntechOpen. https://doi.org/10.5772/intechopen.112652

[40] Zyoud, A., Jondi, W., Mansour, W., Majeed Khan, M. A., & Hilal, H. S. (2016). Modes of tetra(4-pyridyl)porphyrinatomanganese(III) ion intercalation inside natural clays. *Chemistry Central Journal*, *10*(1), 1–9. https://doi.org/10.1186/s13065-016-0153-4